Earthquake Behavior of Cylindrical Underground Structure and Verification of Analytical Model

Takamasa TAKEUCHI
Assistant Manager, Construction Solutions Department, Giken Ltd., Japan
Email: takeuchi@giken.com
Hideo FURUICHI
Procjet Manager, Construction Solutions Department, Giken Ltd., Japan
Email: furuichi@giken.com
Tsuyoshi NISHI
Director, Construction Project Consultants Inc., Japan
Email: t_nishi@cpcinc.co.jp

ABSTRACT

The mechanical advantage of cylindrical underground structures against external forces has been known to many engineers. A cylindrical structure reinforced by intermediate ring beams with hat-shape steel sheet piles as an outer shell is not an exception. However, more discussions are required regarding the behavior study and the design methods at the time of earthquake, since similar structures and their case studies are scarce. With these backgrounds, stresses and acceleration exerted in main structural members have been measured since 2009 under ordinary and seismic conditions, installing measuring instruments inside the structures, and the following points were verified; 1) Based on the acceleration obtained from the actual measurements on structures at the time of the Great East Japan Earthquake (2011), the seismic acceleration waves for a layer equivalent to technical reference base were calculated by means of the ground response analysis. As a result, it was verified that the simulated waves were consistent with the measured results, and that the behavior of the underground structure was in harmony with that of the ground; and 2) Conducting a dynamic analysis based on the seismic acceleration waves calculated in 1), it was verified that the underground structure had a sufficient resistant capacity against an earthquake.

Key words: *cylindrical underground structure, seismic behavior, hat-shape sheet pile dynamic analysis, Great East Japan Earthquake*

1. INTRODUCTION

1.1. Use of underground space in Japan

In Japan, about 70 % of land is occupied by forests, and most of the social infrastructures and population are concentrated in small flat areas, getting close to saturation. Under this social environment, utilizing underground spaces has a great advantage so that it might solve an issue of saturation of various urban functions and creates more leeway. Underground spaces have superior features such as shielding performance, constant temperature and humidity and earthquake resistance, and have been utilized in different fields, such as roads and railways including stations, regulating ponds, lifelines, and vehicle and bicycle parking (Kimura and Kitamura, 2012; ENAA, 2013; Takeuchi and Kimura, 2015). Among the underground facilities described above, our attention has been paid to the facilities for attracting customers such as stations, and the issues specific to urban areas have been identified. It is because there would be more possibilities for proposing facilities with more convenience if underground spaces are utilized. The effects such facilities can provide are also being investigated (Nishikawa and

Takeuchi, 2015).

Illegally parked bicycles due to shortage in parking space have become a social problem around stations and commercial facilities in Japan. These illegally parked bicycles may not only make walking environment worse, but also block emergency activities such as disaster measures and rescue works, and eventually reduce urban functions and spoil scenery. As a solution to the bicycle parking problem, introduced across the country is the ECO Cycle, an automated underground bicycle parking that is space-saving and highly convenient (Takeuchi *et al.*, 2014).

Currently 49 units including ones under construction are introduced in 21 different locations across the country.

1.2. Basic principle in structural design

As this facility, ECO Cycle, has few people in and out at ordinary times, there will be few human damages even when the facility is affected by a major earthquake. For this reason, In the basic principal, the performance under seismic condition has been referred to the Aseismic Performance Ⅰ.

However, it is necessary to consider a possibility of having a damage to the neighboring areas due to deformation of the surrounding ground caused by a large deformation of the main structures at the time of a major earthquake. Therefore, it is essential to examine the behavior of the underground structures and verify the analysis model especially under seismic conditions. Due to such background as this, the inside of the structure has been instrumented since 2009, and the stress and acceleration exerted in the main structures have been monitored both under ordinary and seismic conditions.

This paper presents the results of measurement of this structure at the time of the Great East Japan Earthquake, and those of a dynamic analysis that was performed, where the behavior of underground structures under seismic conditions are taken into consideration.

2. OUTLINE OF STRUCTURE OF AUTOMATED UNDERGROUND BICYCLE PARKING AND ITS CONSTRUCTION METHOD

2.1. Outline of structure

A structural overview of the automated underground bicycle parking facility is shown in **Fig. 1**. ECO Cycle is a cylindrical underground structure that uses hat-shape steel sheet piles (NS-SP-J) with an effective width of 600 mm as the outer shell, reinforced by intermediate ring beams made of H beams. The bottom is made of reinforced concrete, and the floor deck (termed upper floor deck hereinafter) that support entrance/exit booth has a composite slab deck structure supported by H beam steel lattice girders.

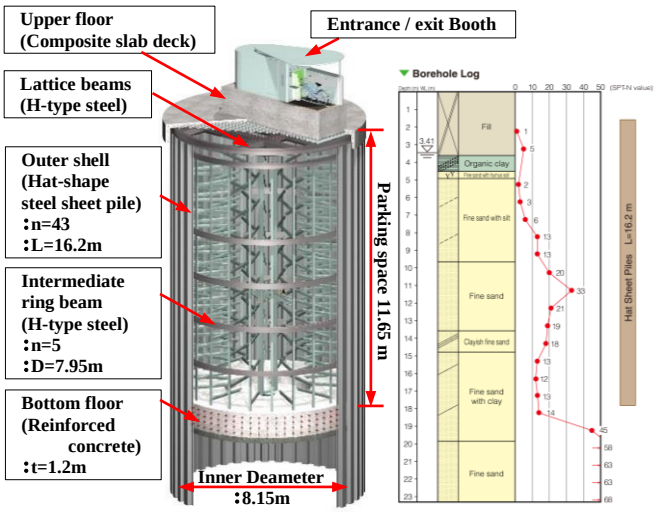

Fig. 1 Structural outline of the bicycle park with the borehole logging results at the planned site

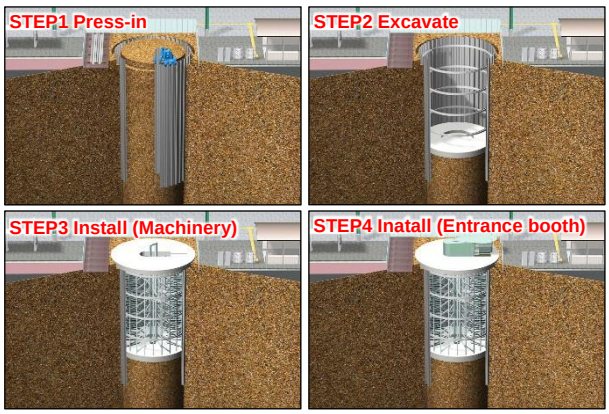

Fig. 2 Construction method

2.2. Outline of construction method

The construction method of this structure is depicted in **Fig. 2**. An outer shell is built, continuously pressing-in 16.2 m-long hat-shape steel sheet piles in a cylindrical shape with inner diameter of 8.15 m. The soil inside the continuous wall is then excavated, and the installation of ring beams and the excavation of inner soil are repeated. Finally, the bottom concrete slab is laid. Consequently, the machine units are installed, the upper floor deck is built, and the facility is completed by installing the entrance/exit

booth. The completed facility is shown in **Fig. 3**.

3. MEASUREMENTS IN UNDERGROUND STRUCTURE

3.1. Measurement device and measurement locations

As shown in **Fig. 4**, measuring instruments such as strain gauges have been installed on the underground structure since the completion of the facility in May 2009.

Six strain gauges were installed on each 1st, 3rd and 5th intermediate ring beam, while the accelerometers (in the N-S and E-W directions) were installed on the 1st and 3rd intermediate ring beams and on the bottom slab floor to verify difference in acceleration with depth. Note that the accelerometer on the bottom floor is not likely to be affected by various vibrations from other parts of the structure, and it was thought that the measurement data at the bottom floor would be very useful in the analysis, by comparing with the accurate seismic vibration.

3.2. Measured items and frequency

Under an ordinary condition, strain is monitored once a day. Considering the effect of normal machine operation on the measurement result, strain was monitored when the frequency of the use of bicycle parking facility was low. Under a seismic condition, on the other hand, once an accelerometer perceives an earthquake with a magnitude larger than 10 gals, all the instruments start automated measurements, with a sampling interval of 0.05 seconds for 180 seconds.

4. MEASUREMENT RESULTS

4.1. Measurement results in normal condition

Fig. 5 depicts the information on the annual change in stress on the intermediate ring beam. Measurement has been continued since May 2009 till now for about 9 years. The reason why the change in stress of the 1st intermediate ring beam is larger than that of the other ring beams is that a temperature correction has been applied to the measured strain, taking into account the temperature change in the underground space. Note that it has been confirmed that the stress has hardly changed from the time of completion till now, indicating that there is hardly any effect by the change in cross sectional area *e.g.*, by corrosion of steel material.

Fig. 3 Perspective view

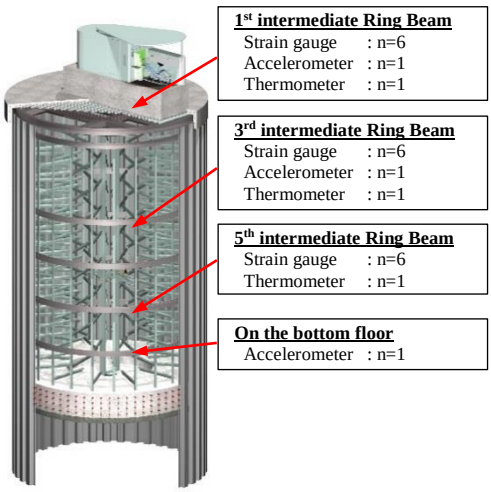

Fig. 4 Measurement instruments and measurement locations

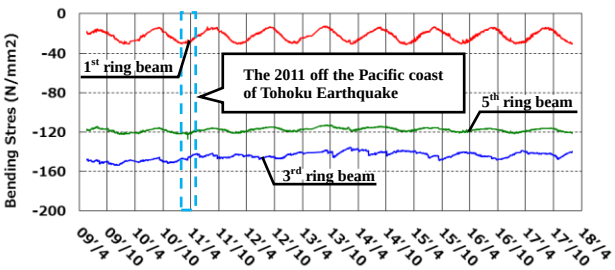

Fig. 5 Change in stress with time (May 2009 - February 2018)

4.2. Measurement results under seismic condition

The Great East Japan Earthquake that took place on March 11, 2011 recorded the maximum seismic intensity of 7 in the Richter scale in Kurihara, Miyagi Prefecture, Japan, and 5+ in this project site. **Fig. 6** shows the acceleration recorded on the 1st ring beam of the structure, indicating the maximum response of 172 gals in the N-S direction. The acceleration response measured became larger as the measurement point became closer to the ground surface, verifying that the measurement data are in good order.

4.3. Comparison of results between normal and seismic conditions

Table 1 shows the measured and allowable stresses of the ring beam under ordinary and seismic conditions. It may be seen that the values in the table are measured maximum stresses, and that they are all within the allowable stresses.

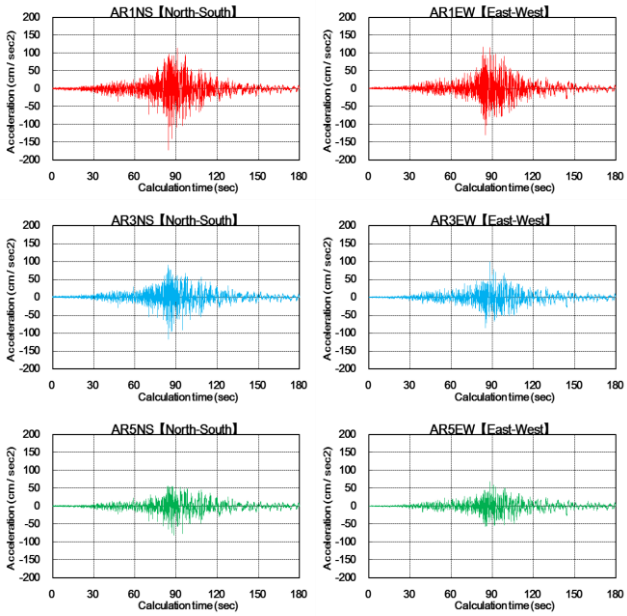

Fig. 6 Acceleration obtained

Table 1. Measured stress and allowable stress of the ring beams under ordinary and seismic conditions

Bending Stress (N/mm^2)	Originary (※1)	Seismic (※2)	※2 - ※1	Allowable Stress (N/mm^2)
1st Ring beam	29.5	29.4	-0.1	156 (235)
3rd Ring Beam	148.3	152.2	4.0	216 (325)
5th Ring Beam	121.8	141.8	19.9	216 (325)

5. OUTLINE OF VERIFICATION

5.1. Verification principle

Based on the measured acceleration, a simulation analysis was carried out, calculating seismic acceleration waves on the layer equivalent to the technical reference base by the earthquake response analysis. After confirming that the measured results were represented well in the simulation, the applicability of the analysis model was evaluated.

Using the same analysis model and inputting Level 2 earthquake, the behavior against the earthquake at this level was then predicted. Based on the prediction results, the resistance capacity of each member was investigated in detail, and the safety against Level 2 earthquake was evaluated.

5.2. Outline of analysis model

The analysis model of this structure is shown in **Fig. 7**. The outer shell and the intermediate ring beams are modelled by beam elements, while the bottom slab and the upper floor deck are modelled by plate elements. Since the outer shell is formed by interlocking hat-shape steel sheet piles including interlocks which are not rigid, the connection between piles are slightly flexible. Therefore, the outer shell was not modelled by plate elements, but by independent beam elements where relative displacements

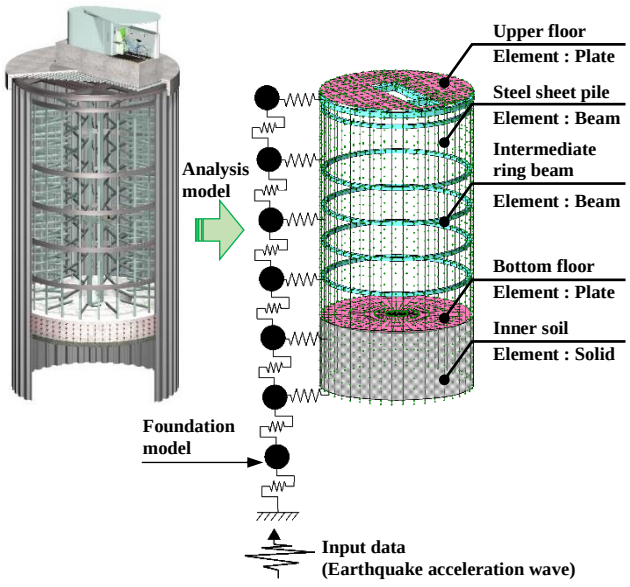

Fig. 7 Schematic view of analysis model

were allowed between steel sheet piles. The upper floor deck is used to transfer surcharge load, but was modelled in such a way that its behavior could be as realistic as possible. The lattice girder by H-shape steel and the upper

deck composite slab were modelled by the beam and plate elements at the same time. The ground below the bottom slab which was confined by the outer shell was modelled by the solid element.

In addition, as shown in **Fig. 7**, since the earthquake analysis was dynamic, a one-dimensional ground model (solid ground model in reality) was made, and this ground model was connected with the structure model with ground springs.

The actual model is shown in **Figs. 8 and 9**. **Fig. 8** is an entire analysis model, and the ground is modelled as solid ground, and is connected with the structure using the ground springs. **Fig. 9** shows the model without the ground springs, while the ground is modelled by multi-layer model. Stiffness of each soil layer is determined by the converged stiffness in separately performed one-dimensional ground response analysis by an analysis code "SHAKE". The dynamic analysis itself is carried out as a linear analysis. Note that the stiffness and mass of the ground was assumed 10^5 times larger than that of normal ground, so that the response of the structure would not affect the ground response.

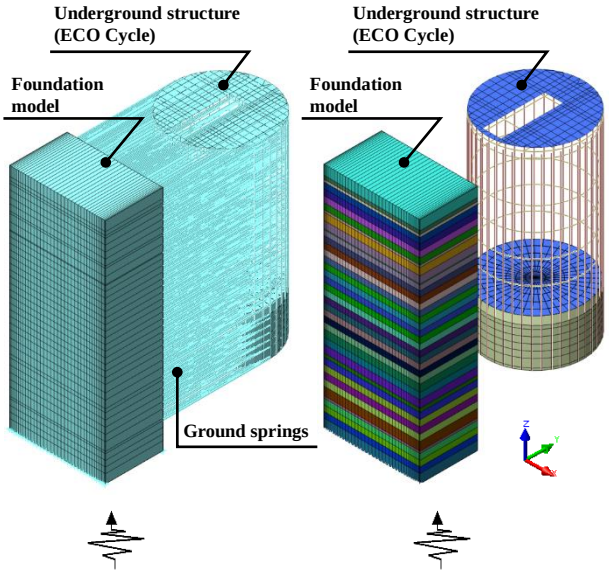

Fig. 8 Overall analysis model

Fig. 9 Analysis model (without spring)

6. SEISMIC TREMOUR FOR CONSIDERATION

6.1. Simulation analysis

As for the earthquake for evaluation, an earthquake on the technical reference base was set up based on the records from the accelerometer installed on the bottom slab of the underground structure (**Fig. 6**). That is to say, it was assumed that the bottom slab was rigid, and that the measured acceleration was the same as that of the ground. Based on this assumption, in the ground response analysis by "SHAKE", the acceleration measured on the bottom slab was applied to the ground at a depth where the accelerometer was installed, and the seismic acceleration wave was calculated in the layer equivalent to the technical reference base. Thus-calculated acceleration was used as input data. The earthquake acceleration wave was applied at the same time in the X- and Y-directions.

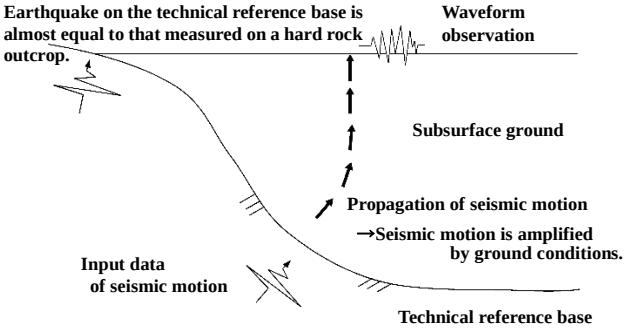

Fig. 10 Earthquake on the technical reference base

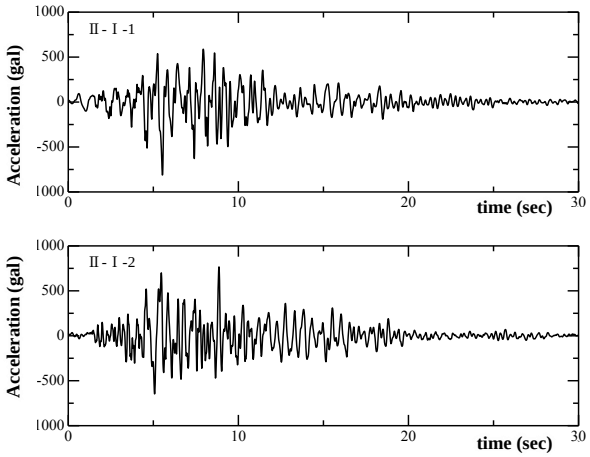

Fig. 11 Type I ground wave, Chapter V, Guideline for road bridges)

6.2. Level 2 earthquake

The earthquake on a layer equivalent to the technical reference base is not prescribed in the existing guidelines such as the specifications for highway bridges in Japan. In this evaluation, assuming that the earthquake on the technical reference base is equal to that measured on a hard rock outcrop, and the earthquake acceleration wave prescribed for the type I hard ground is used as input data (**Fig. 10**).

Fig. 11 shows the earthquake acceleration wave. As

shown here, 2 type-II waves II-1-1 and II-1-2 are selected among those in Level 2 earthquakes in Chapter V of the specifications for highway bridges (JRA, 2012). These waves are spectrum-adjusted from the seismic waves in the N- and E-directions observed at the Kobe Marine Observatory at the time of the Hyogo-ken Nanbu Earthquake in 1995.

6.3. Ground condition

The ground condition is summarized in **Table 2**. The shear wave velocity shown in the table is from the relationship by Imai et al. shown in **Fig. 12**. The standard curves shown in Materials 1504 and 1778 of the Public Works Research Institute (PWRI) of the Ministry of Land, Infrastructure, Transport and Tourism are used to describe non-linear features of the ground.

6.4. Converged physical properties by ground response analysis

As described previously, the converged values in the ground response analysis by a code "SHAKE" are used for the physical properties of the ground used in the dynamic analysis.

Note the spring constant of the ground may be calculated using the following equation (Kawashima, 2011):

$k_n = 2G / R$, $k_s = k_n / 3$

k_n: Spring constant in normal direction (kN / m^3)

k_s: Spring constant in tangential direction (kN / m^3)

R: Radius of the structure (m)

G: Elastic Shear modulus of ground (kN / m^2)

7. ANALYSIS RESULTS

7.1. Comparison of response values in simulation analysis

The record of measured acceleration on the bottom slab (ADN) in the N-direction is shown in **Fig. 13**, while the calculated result at the same location is shown in **Fig. 14**. Furthermore, the both results are superimposed and compared in **Fig. 15**, extracting the values at the time between 80 and 90 seconds, where acceleration is rather big. It may be seen that the calculated acceleration at the 1st ring beam is rather high, but that the calculated and measured values are relatively in good agreement.

Similarly, the measured and calculated acceleration values are compared in **Fig. 16** in the E-direction. As in the N-direction, calculated values are in good agreement with the measured values. It is therefore judged that the analysis could simulate the measurement results.

Table 2. Ground Condition

Strata	Altitude	Layer	N	γ	Vs	G_0	v	h_0	Remarks
				kN/m3	m/s	kN/m2			
Fill	6.020								
	5.195	0.825	3	19.0	116	26,065	0.45	0.01	
	4.895	0.300	3	19.0	116	26,065	0.45	0.01	
	4.690	0.205	3	19.0	116	26,065	0.45	0.01	
	4.190	0.500	3	19.0	116	26,065	0.45	0.01	Sheet pile top
	3.663	0.527	3	19.0	116	26,065	0.45	0.01	1st Ring beam
	3.137	0.526	3	19.0	116	26,065	0.45	0.01	
	2.610	0.527	3	19.0	116	26,065	0.45	0.01	
	2.420	0.190	3	19.0	116	26,065	0.45	0.01	
Organic clay	1.805	0.615	3	13.0	141	26,215	0.49	0.01	
	1.190	0.615	3	13.0	141	26,215	0.49	0.01	
	1.120	0.070	3	13.0	141	26,215	0.49	0.01	
Fine sand with silt	0.690	0.430	14	17.0	193	64,659	0.49	0.01	2nd Ring beam
	0.190	0.500	14	17.0	193	64,659	0.49	0.01	
	-0.310	0.500	14	17.0	193	64,659	0.49	0.01	
	-0.810	0.500	14	17.0	193	64,659	0.49	0.01	
	-1.310	0.500	14	17.0	193	64,659	0.49	0.01	3rd Ring beam
	-1.810	0.500	14	17.0	193	64,659	0.49	0.01	
	-2.310	0.500	14	17.0	193	64,659	0.49	0.01	
	-2.810	0.500	14	17.0	193	64,659	0.49	0.01	
	-3.310	0.500	14	17.0	193	64,659	0.49	0.01	4th Ring beam
	-3.810	0.500	14	17.0	193	64,659	0.49	0.01	
	-4.310	0.500	14	17.0	193	64,659	0.49	0.01	
	-4.810	0.500	14	17.0	193	64,659	0.49	0.01	
	-5.310	0.500	14	17.0	193	64,659	0.49	0.01	5th Ring beam
	-5.810	0.500	14	17.0	193	64,659	0.49	0.01	
	-6.310	0.500	14	17.0	193	64,659	0.49	0.01	
	-6.930	0.620	14	17.0	193	64,659	0.49	0.01	
	-7.480	0.550	14	17.0	193	64,659	0.49	0.01	Bottom floor
Fine sand with clay	-8.130	0.650	19	19.0	252	122,726	0.49	0.01	
	-8.430	0.300	19	19.0	252	122,726	0.49	0.01	
	-8.975	0.545	19	19.0	252	122,726	0.49	0.01	
	-9.520	0.545	19	19.0	252	122,726	0.49	0.01	Ground improvement
	-10.065	0.545	19	19.0	252	122,726	0.49	0.01	
	-10.610	0.545	19	19.0	252	122,726	0.49	0.01	
	-11.330	0.720	19	19.0	252	122,726	0.49	0.01	
	-11.510	0.180	19	19.0	252	122,726	0.49	0.01	Sheet pile tip
	-12.010	0.500	19	19.0	252	122,726	0.49	0.01	
	-12.510	0.500	19	19.0	252	122,726	0.49	0.01	
	-13.010	0.500	19	19.0	252	122,726	0.49	0.01	
	-13.780	0.770	19	19.0	252	122,726	0.49	0.01	
Foundation				20.0	300				

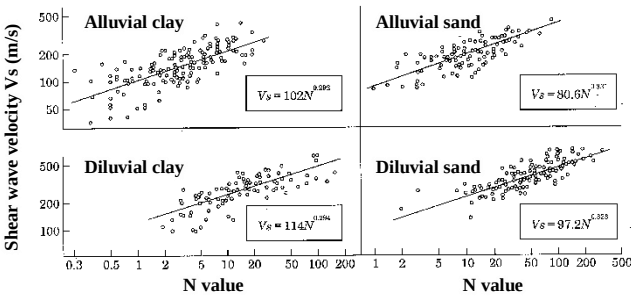

Fig. 12 Relationship between shear wave velocity Vs and N-value (Imai *et al.*, 1977)

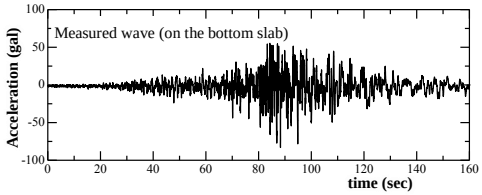

Fig. 13 Measured wave of seismic acceleration (N-direction)

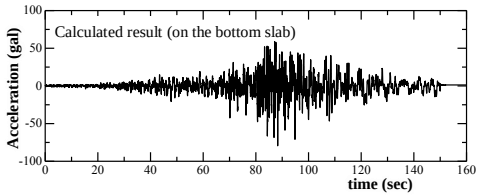

Fig. 14 Calculated result of seismic acceleration (N-direction)

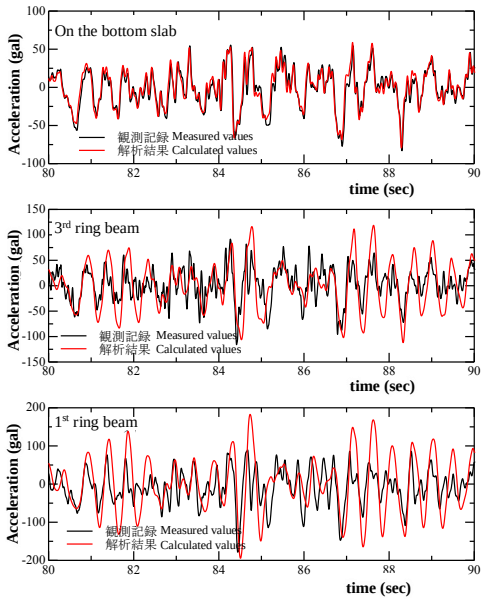

Fig. 15 Comparison of measured and calculated values (N-direction)

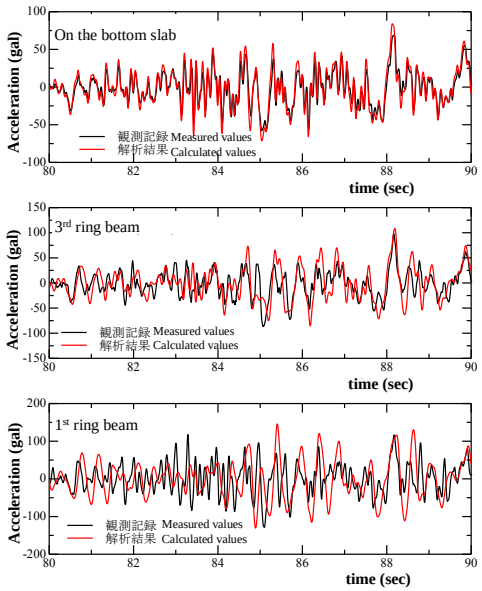

Fig. 16 Comparison of measured and calculated values (E-direction)

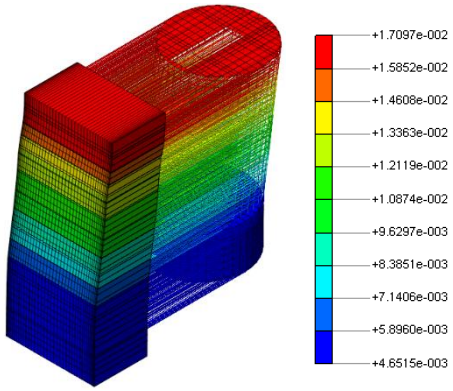

Fig. 17 Maximum resultant displacement obtained from simulation analysis (unit:m)

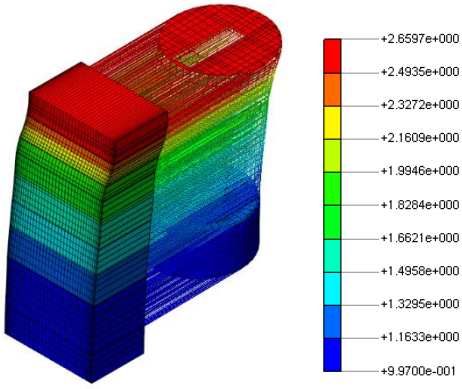

Fig. 18 Distribution of maximum resultant acceleration obtained from simulation analysis (unit:m)

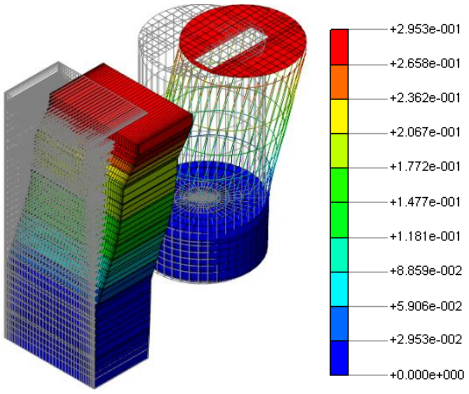

Fig. 19 Maximum resultant displacement under Level 2 earthquake(unit:m)

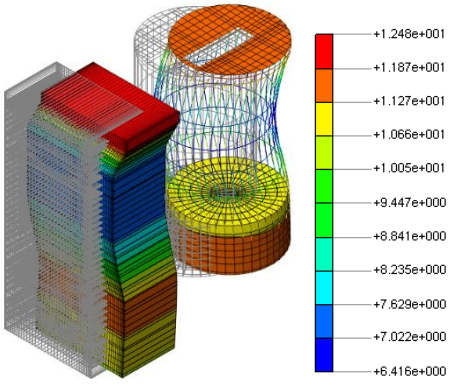

Fig. 20 Distribution of maximum resultant acceleration under Level 2 earthquake (unit:m)

7.2. Distributions of deformation, acceleration and cross-sectional force in simulation analysis

The maximum displacements are shown in **Fig. 17**. In the figure, relative values to the input base of the earthquake are shown, and the maximum displacements are resultant values in the X-, Y- and Z-directions. The maximum resultant displacement is 17.1 mm, and this is consistent with the maximum forced deformation of 16.7 mm calculated by a static response deformation method for the same model. **Fig. 18** shows the distribution of maximum acceleration. The maximum resultant acceleration was 266 cm/s^2 at the top of the structure. The cross sectional forces are summarized in **Table 3**. It may be seen that neither intermediate ring beams nor hat-shape steel sheet piles show large stress increments.

7.3. Comparison between measurement and simulation analysis

Table 4 compares the measured and calculated stress increments of the ring beam at the time of earthquake. It may be seen that the calculated values are somewhat smaller than those measured. It may be because the analysis is concerned with earthquakes in the horizontal direction only, and the ground and structures were modelled in a simplified ideal condition. Note that the differential stress is only several percent of the yield stress, and it is judged that there will be no problem.

7.4. Distributions of deformation, acceleration and cross-sectional force under level 2 earthquake

The maximum displacement is shown in **Fig. 19**, while the maximum resultant displacement is 295 mm at the top of the structure, suggesting that large stress is acting on the structure. **Fig. 20** shows the distribution of the maximum acceleration. The maximum resultant acceleration was 1,248 cm/sec^2 at the top of the structure.

Table 5 summarizes the cross-sectional forces. Though there were no large stress increments on the intermediate ring beams, they were large in the hat-shape steel sheet piles.

Table 3. Calculated sectional force in the simulation analysis

Member	Unit	Ring beams H-200×200×8×12	Hat-shape steel sheet pile
Cross sectional area	m2	6.35E-03	9.45E-03
Moment of inertia of area	m4	4.72E-05	6.16E-05
Section modulus	m3	4.72E-04	5.99E-04
Maximum bending moment	kNm	4.36E-01	1.15E+01
Bending stress	N/mm2	9.24E-01	1.92E+01
Maximum axial force	kN	3.14E-01	–
Stress due to axial force	N/mm2	4.95E-01	–
Maximum shear force	kN	4.86E-01	1.77E+01
Shear stress	N/mm2	7.65E-02	1.88E+00

Table 4. Comparison between measured and calculated values

Bending Stress (N/mm^2)	Measurement (※1)	Analysis (※2)	※2 - ※1
1st Ring beam	-0.1	-0.7	-0.5
3rd Ring Beam	4.0	0.8	-3.1
5th Ring Beam	19.9	4.3	-15.6

Table 5. Calculated sectional force under Level 2 earthquake

Member	Unit	Ring beams H-200×200×8×12	Hat-shape steel sheet pile
Cross sectional area	m2	6.35E-03	9.45E-03
Moment of inertia of area	m4	4.72E-05	6.16E-05
Section modulus	m3	4.72E-04	5.99E-04
Maximum bending moment	kNm	8.01E+01	1.05E+02
Bending stress	N/mm2	1.70E+01	1.75E+02
Maximum axial force	kN	2.35E+02	–
Stress due to axial force	N/mm2	3.69E+01	–
Maximum shear force	kN	7.05E+00	1.57E+02
Shear stress	N/mm2	1.11E+00	1.66E+00

8. SUMMARY

In this paper, the underground structure was overviewed, the contents of measurements were described, and the measured and calculated results of the behavior at the time of earthquakes were compared. Judging from the measurement results, it was proven that the underground structure possessed sufficient aseismic performance for earthquakes with the intensity of about 5+. The facility referred to for this paper is revisited in **Fig. 21**. From the results of a dynamic analysis using the measurement results, as previously predicted, it was confirmed that the structure would behave harmoniously with the ground, and a useful set of data were obtained. In addition, as a result of verifying the behaviour calculated in the analysis with the same analysis model under Level 2 earthquake, main members did not reach the yielding point. It was therefore concluded that the structure possessed sufficient aseismic performance and would not fail under the Level 2 earthquake.

Lately, interest in the aseismic performance of the structures has been rapidly increasing. In addition, from the features of installation location of the underground structures, the constructions adjacent to important structures such as railway structures have an increasing trend in number. As an example, **Fig. 22** introduces a case study adjacent to a railway track and a bridge pier of a viaduct of a bullet train line. The construction was only 13 m away from the bridge pier of the viaduct. The structures and construction methods that would not affect the neighboring area were required to be finally adopted.

With the revision of the Guideline for the Road Bridges, the design method is shifting from the conventional specification type to the performance provision type, and it is necessary to propose more suitable structures and analysis methods for the underground structures. In addition, with the revision of the guideline, the design in-service period is prescribed to be 100 years as a standard. Implementation of suitable maintenance during this period is also prescribed. The measurement method described in this paper uses automated and remote-controlled data acquisition from the instruments installed in the underground structures and contributes to labour-saving in maintenance works. In future, we will carry out more suitable maintenance work using continuous measurements and develop more accurate analysis methods.

Fig. 21 Photo after completion of the facility

Fig. 22 Excavation of inner soil (construction status)

REFERENCES

Engineering Advancement Association of Japan (ENAA). 2013. A Guide to develop Underground Space Utilization and Planning. (in Japanese)

Japan Road Association (JRA). 2012. Specifications for Highway bridges, Part V: Seismic Design. (in Japanese)

Kawashima, K. 2011. Aseismic design of underground structures, Kajima Publishing Co. (in Japanese)

Nishikawa, K. and Takeuchi, T. 2015. Effect of measures against illegally parked bicycles at the South Exit of the Shinagawa Station, Japan Road Conference, June 2015. (in Japanese)

Public Works Research Institute (PWRI) of the of the Ministry of Land. 1979. Infrastructure, Transport and Tourism, Materials 1504.

Public Works Research Institute (PWRI) of the of the Ministry of Land. 1982. Infrastructure, Transport and Tourism, Materials 1778.

Takeuchi, T., Furuichi, H. and Nishi, T. 2014. Verification of dynamic behavior of an underground mechanical bicycle park during earthquake with numerical model, Proceedings of the 69th JSCE annual assembly. (in Japanese)

Takeuchi, T. and Yasumasa, K. 2015. Effective Utilization of Underground Space in Urban Area, 15th Asian Regional Conference on Soil Mechanics and Geotechnical Engineering.

Yasumasa, K. and Akio, K. 2012. Underground Mechanical Car Parking Facilities/Foundations, World Conference of Associated Research Centers for the Urban Underground Space (ACUUS 2012).